PAPER

An angle sensor based on a sector ring patch antenna for bolt loosening detection

To cite this article: Chunfeng Wan *et al* 2022 *Smart Mater. Struct.* **31** 045009

IOP Publishing Smart Materials and Structures
Smart Mater. Struct. **31** (2022) 045009 (11pp) https://doi.org/10.1088/1361-665X/ac55d9

An angle sensor based on a sector ring patch antenna for bolt loosening detection

Chunfeng Wan[1], Zhiquan Zheng[2], Songtao Xue[2,3], Liyu Xie[2,*] and Guochun Wan[4]

[1] Key Laboratory of Concrete and Pre-stressed Concrete Structure of Ministry of Education, Southeast University, Nanjing, People's Republic of China
[2] Department of Disaster Mitigation for Structures, Tongji University, Shanghai, People's Republic of China
[3] Department of Architecture, Tohoku Institute of Technology, Sendai, Japan
[4] Department of Electronic Science and Technology, Tongji University, Shanghai, People's Republic of China

E-mail: liyuxie@tongji.edu.cn

Received 12 October 2021, revised 8 February 2022
Accepted for publication 16 February 2022
Published 25 February 2022

Abstract

This paper presents an angle sensor based on a sector ring patch antenna (SRPA) for loose bolt detection. The sensor is comprised of two parts, a ring substrate sandwiched between a ground plane and a sector ring radiation patch, and a sector ring substrate covered by a radiation patch. The two radiation patches are partially overlapped and the overlapped areas are in contact allowing the electric current to flow within the combined radiation patch. The resonant cavity theory is adopted to explain the relationship between the frequency shift and the overlapped angle. The Ansoft high frequency structure simulator software is used to simulate SRPA, and the dimensional parameters of the antenna are optimized to make the antenna perform better. For verification, two sets of SRPAs are fabricated and tested.

Keywords: structural health monitoring, bolt loosening detection, antenna sensor, sector ring patch antenna

(Some figures may appear in colour only in the online journal)

1. Introduction

Bolt connections are widely used in many industries, including mechanical engineering, civil engineering and aerospace engineering. Their popularity is due to easy installation and implementation, the ability to bear relatively heavy loads, low costs, and acceptable reliability [1]. However, under the influence of temperature fluctuation, repeated forces, and vibrations, bolt threads tend to slip relative to the joint threads, leading to bolt loosening [2]. If the loose bolts cannot be found and retightened in time, the bolt connection with the loose bolts will be a weak point of the structure, threatening the safety of the whole structure.

Generally, it takes some time for bolts to be completely loosened from tightening state, which generally undergoes two steps. Firstly, the decrease of early preload results in the decrease of the frictional forces at bolt interface. Then, due to the plastic deformation of threads, the micro-slip between contact surfaces and the creep phenomenon, the relative movement occurs between the fastener and the connection [3]. Therefore, to prevent accidents caused by bolt loosening in a timely manner, some traditional methods, which mainly utilize strain gauges, stress sensors, or the torque wrench technique [4] were developed in industries. Technologies based on strain gauges or stress sensors are relatively expensive and

* Author to whom any correspondence should be addressed.

have difficulty achieving high accuracy. As another traditional monitoring method, torque wrench technology is currently used in many and various structures. Nevertheless, this method has a wide error of up to 50% [5]. And, the accuracy behind the use of this technology is affected by the professional level of the inspector.

Then, with the development of technology and smart materials, some attractive approaches, such as impedance-based, vibration-based, and ultrasonic-based methods, have been proposed. The impedance-based methods [6, 7] interrogate the electromechanical impedance's variation of bolt connections stimulated by piezoelectric transducers, which behave differently depending on whether the bolts are tightened or loosened. Vibration-based approaches [8–10] use hammers, vibrators, piezoelectric elements, or other ways to vibrate the bolted structure and record the dynamic response through piezoelectric accelerometers or laser vibrometers. The recorded data are then analyzed to obtain the structure's vibration parameters. That structure's vibration characteristics are the basis for estimating the bolt loosening state. In the ultrasonic-based method category, the changes in ultrasonic waves sent to bolt connections are examined as an index for the existence of flaws. The method mainly includes piezoelectric active sensing methods [11, 12] the acoustoelastic effect-based methods [13] and the emergence of harmonics-based methods [14]. However, most of the techniques mentioned above require sensors to be placed on or near the bolts, which commonly require high-precision instrumentation that has difficulty compensating for the complex environmental effects.

To offset the disadvantages of the methods mentioned above, researchers have proposed many novel bolt loosening detection methods. Among them, image processing-based methods are gaining significant momentum [2, 15]. Combined with machine learning algorithms, image processing-based methods can realize the automatic monitoring of bolt loosening. The pros of this method are that its investigation results are minimally affected by environmental noise and can be analyzed qualitatively and tangibly. However, it does have lighting or no-covering requirements for image capturing. In conditions where digital cameras have difficulty obtaining structural images due to heavy fog conditions, poor lighting, or the covering material on the bolts, the application of this method is limited. It is also very changeling to acquire stable bolts images on a rotating or reciprocating object.

An approach based on radio wave interrogation can circumvent the problem of image processing-based methods commendably. In 2016, Wu *et al* [16] proposed a way to use radio-frequency identification (RFID) technology to monitor the rotation of bolts or nuts. Using electromagnetic waves to transmit signals that are unaffected by light conditions, this method can work in dimly lit coal mines. However, due to the installation limitations due to the form of coal mine guide structures, this method can only observe the bolt loosening in a specific application when the nut's rotational angle exceeds 20°. In addition, this method can only judge whether the bolt is loose qualitatively. In order to judge the state of bolts more accurately, some new approaches are urgently needed to remedy this deficiency and even realize the quantitative judgment of the bolt status. Patch antenna-based sensors, which are commonly used for quantitative strain or crack monitoring in the field of structural health monitoring, have attracted our attention due to their advantages such as simple configuration, multimodality, and low cost [17, 18].

Initially, patch antenna sensors were primarily monolithic, pasted on the surface of structures to measure the strain [19, 20] or cracks [21]. And Yi *et al* [22] extended its usage to monitor the setting time in cement hydration. However, stressed single-patch antenna sensors are facing some disadvantages, such as, incomplete strain transfer ratio and insufficient strength [23]. Thus, an unstressed patch antenna sensor has been proposed to avoid the problems confronted by stressed single patch antenna sensors. In 2019, Xue *et al* [24] introduced their newly developed rectangular patch antenna with an overlapping sub-patch for crack monitoring. Later, Xue *et al* [25] applied this antenna sensor with an overlapping sub-patch to detect changes in the length of screw and thus identify the bolt loosening activity. Inspired by the idea of unstressed patch antennas, this paper proposes a sensor based on unstressed patch antennas for monitoring angle rotation, which is a sector ring patch antenna (SRPA) used to monitor the rotation of nuts that occurs during the second stage of bolt loosening.

The SRPA is composed of two parts: (a) a ring substrate sandwiched between a ground plane and a sector ring radiation patch and (b) a sector ring substrate with a same-shaped radiation patch. The two radiation patches' partially overlapped parts are in immediate contact with each other, and together, they form the antenna's sensing part. When properly mounted on the bolt connection, the rotation of the nut will cause the sector ring substrate to simultaneously rotate against the ring part, thereby changing the resonant frequency of the antenna. By analyzing the variations in resonant frequency obtained through a reader, the condition of the bolt connection can be inferred.

The main contents of the following chapers are as follows: section 2 introduces the design and sensing principle of the SRPA. Section 3 presents the sensor model and numerical simulation results. Section 4 focuses on the experimental instrumentation setup and compares the simulation results with the experimental results. Conclusions are then drawn, and future research potential is discussed.

2. Design and theory

Temperature fluctuations, repeated forces and vibrations, which over time cause the bolt's nut to slowly rotate relative to the screw, leading to eventual bolt loosening [2]. Therefore, monitoring the early rotation of the nut can catch the signs of bolt loosening in time. This is an effective indirect bolt loosening monitoring method. Other methods have been proposed. Huynh *et al* [2] were able to detect a loosened bolt with a rotation of 2.74° for a perspective angle of $\leqslant$10°. They were also able to detect a loosened bolt with a rotation of 5.14° for a perspective angle of 40°. However, when the angle went above 40°, accuracy decreased substantially. Wu *et al* [16] designed

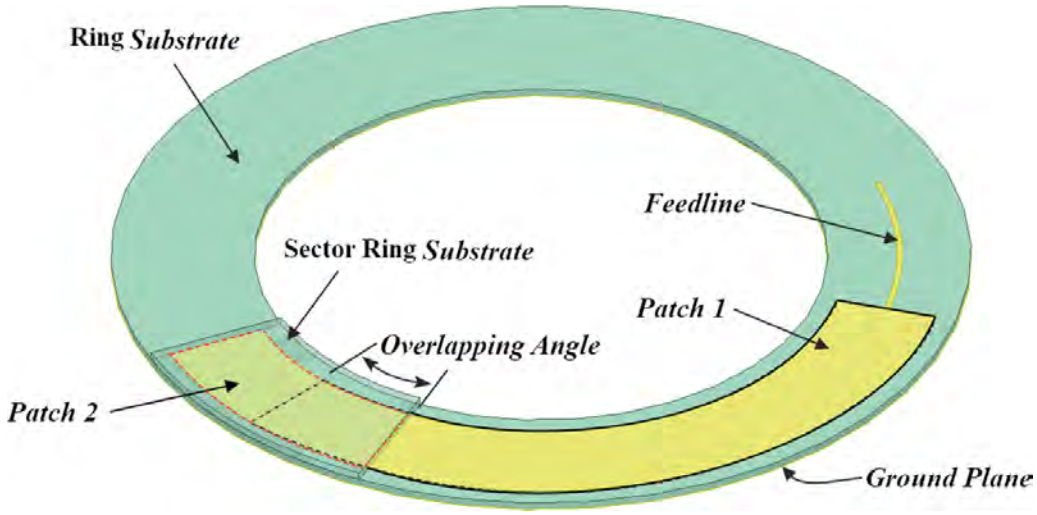

Figure 1. Components of the SRPA.

a device with an RFID patch to detect loosening of bolts. However, the method can only detect loosening of a bolt when its nut is rotated more than 20°. In order to detect the early bolt loosening more accurately and in a more timely manner, we propose a novel angle sensor based on a SRPA.

2.1. Design

The SRPA with two dielectric substrates is shown in figure 1. To fully express the structure of the antenna, the sector ring substrate in the figure 1 is made translucent. The lower surface of the ring substrate is covered with copper as a ground plane, and its upper surface is printed with a sector ring patch (Patch 1) and feedline. Meanwhile, a same-shaped patch (Patch 2) is printed on the lower surface of the sector ring substrate. The sector ring substrate is placed on the ring substrate. Patch 1 and Patch 2 are in contact with each other, and the angle of the overlapping part is represented by the variable α_{ol}. At this point, the radiation patch of the antenna can be regarded as a sector ring patch composed of Patch 1 and Patch 2. The center angle of the radiation patch is the sum of the central angles of Patch 1 and Patch 2 minus the center angle of the overlapping part of the two patches. As the sector ring substrate rotates around its center, the angle of the overlapping part changes, which changes the antenna's resonant length and resonant frequency. The sensing principle is similar to the rectangular patch antenna with an overlapping sub-patch proposed by Xue *et al* [24].

When using the bolt loosening monitor, the ring substrate is fixed to the steel block through adhesive, and the sector ring substrate is connected to the nut through a connection with a hexagonal opening, as shown in figure 2. The shape and size of the opening in the middle of the connection can vary according to the nut. The rotation of the nut causes the rotation of the sector ring substrate, which changes the antenna's resonant frequency. By monitoring the change of the SRPA's resonant frequency, the rotation of the nut can be sensed.

2.2. Theory

According to the resonant cavity theory for a normal rectangular patch antenna, assuming the electric length is L and the electric width is W, the resonant frequency can be calculated as [26]:

$$f_{\mathrm{mn}} = \frac{c}{2\pi\sqrt{\varepsilon_r}}\sqrt{\left(\frac{m\pi}{L}\right)^2 + \left(\frac{n\pi}{W}\right)^2} \tag{1}$$

where m and n are the order in the longitudinal direction and transverse direction, respectively. c is the speed of light, ε_r is the dielectric constant of the dielectric substrate, f_{mn} is the resonant frequency when the antenna is resonant at m orders in a longitudinal direction and when the antenna is resonant at n orders in the transverse direction.

The upper patch of the SRPA can be considered as a variant of the rectangular patch. Since the rotation of the upper substrate only changes the peripheral length of the equivalent radiation patch, it is sufficient to focus on the resonance of the peripheral direction. The resonant frequencies of the peripheral direction can be calculated as:

$$f_{\mathrm{m0}} = \frac{mc}{2L\sqrt{\varepsilon_r}} \tag{2}$$

where f_{m0} represents the resonant frequency of order m in the peripheral direction, and L represents the equivalent peripheral length of the radiation patch of the antenna. Then, L can be expressed as:

$$L = 2\pi R\frac{\alpha_e}{360} \tag{3}$$

where R represents the equivalent radius of the sector ring patch (R), and α_e represents the central angle of the effective part of the two sector ring patches. The central angle of the effective part of the sector ring patch α_e can be represented by the sum of the central angles of Patch 1 and Patch 2 (α_t) and the overlapping angle between them (α_{ol}):

$$\alpha_e = \alpha_t - \alpha_{\mathrm{ol}}. \tag{4}$$

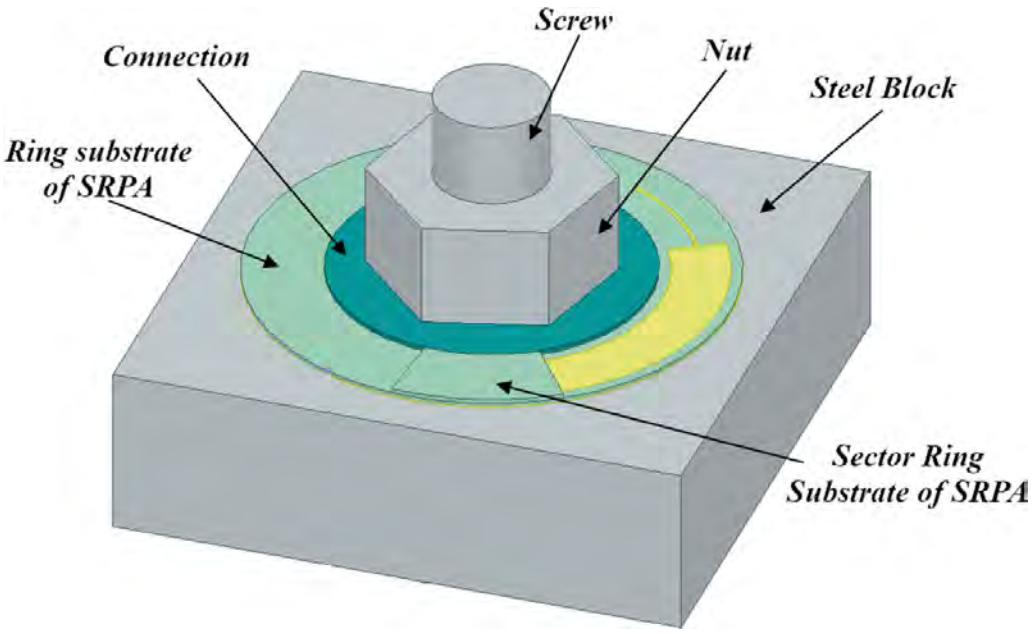

Figure 2. Installation diagram of the SRPA.

Based on the above three equations, as the overlapping angle between Patch 1 and Patch 2 decreases, the first three order resonant frequencies of the SRPA will increase, and vice versa. When the change of L is small enough, that is, the change of the overlapping angle between Patch 1 and Patch 2 is small enough, the change in the resonant frequency of SRPA and the change in L shows a linear relationship approximatively. As shown in the following equation:

$$\Delta f_{\mathrm{m0}} = -\frac{mc}{2L^2\sqrt{\varepsilon_r}}\Delta L \tag{5}$$

where Δf_{m0} is the change of the resonant frequency, and ΔL represents the change of the effective length of the radiation patch in the peripheral direction.

3. Simulation

In this section, the electromagnetic properties of the proposed SRPA are simulated using the high frequency structure simulator (HFSS) (Ansoft Corp., 2005). The model of the SRPA consists of two parts: (a) a ring dielectric substrate sandwiched between a sector ring radiation patch (Patch 1) with a feed line and a ring ground plane and (b) a sector ring dielectric substrate with a same-shaped radiation patch (Patch 2). The dielectric substrates and radiation patches of the two parts have the same radial width. The side of the sector ring substrate with the radiation patch is placed downward on the ring substrate, ensuring that the radiation patches of the two parts are in contact with each other, as shown in figure 3. The dielectric substrate material is FR4 with a dielectric constant of 4.4. Both the radiation patches and the ground plane are made of copper. The sensing system is located in an air cylinder whose boundary is more than a quarter of a wavelength away from the SRPA model to ensure computational accuracy of the far-field radiation. The air cylinder serves as radiation boundaries. The ground plane and the radiation patches are set as perfect E boundaries to make the electric field perfectly perpendicular to the surfaces. At the end of the feed line, a lumped port connected to the ground plane is arranged to feed the antenna.

After a series of simulation, with the returen loss of the third-order resonant frequency at peripheral direction as the main index, a group of antennas with better performances was selected. The dimension parameters of the selected antenna are shown in table 1, and the schematic diagram of each parameter is shown in figure 4.

3.1. Verification of theory

The current diagram of the first three orders resonance of the SRPA obtained by numerical simulation is shown in figure 5. According to figure 5, the first three antenna resonances are circumferential. The current distribution of the antenna is similar to that of a regular rectangular patch antenna. Therefore, the theory of the rectangular patch antenna is a good fit for the SRPA.

3.2. Performance simulation

HFSS (Ansoft Corp., 2005) was used to simulate the change of resonant frequency of the SRPA caused by the rotation of the sector ring substrate. Figure 6 shows the results (the S11 curves). As the overlapping angle between Patch 1 and Patch 2, (α_{ol}) changes from 0° to 40°, the third-order resonant frequency of the SRPA increases gradually.

From the S11 curves, the third-order resonant frequencies corresponding to different overlapping angles between Patch 1 and Patch 2 (α_{ol}) are extracted, as shown in figure 7. Through simulation results and data fitting, the value of the

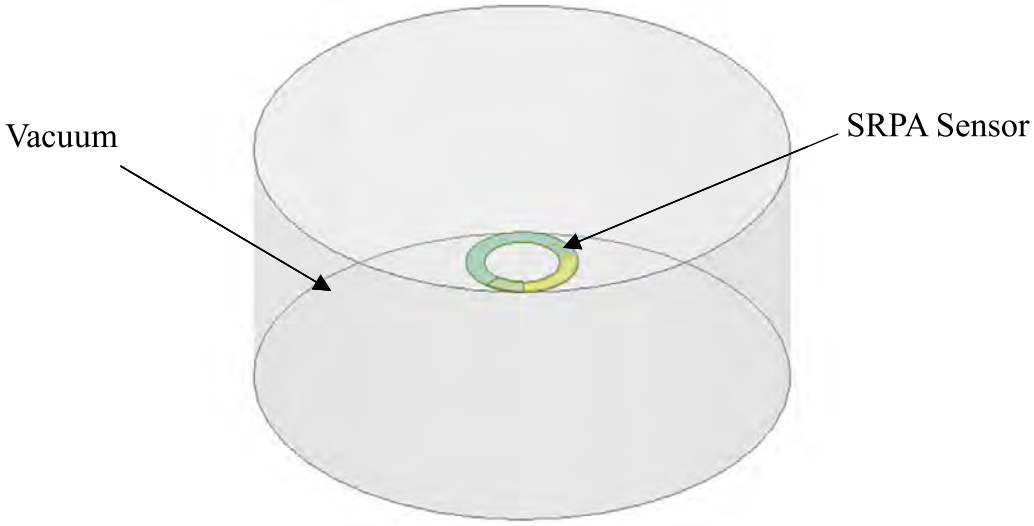

Figure 3. Schematic diagram of the SRPA.

Table 1. Dimension parameters of the chosen group.

R_{s1}	R_{s2}	R_{p1}	R_{p2}	R_{fl1}	R_{fl2}	α_{p1}	α_{fl}	α_{p2}	t
28 mm	42 mm	30 mm	40 mm	35.25 mm	34.75 mm	120°	35°	40°	0.8 mm

t is the thick of the two dielectric substrates.

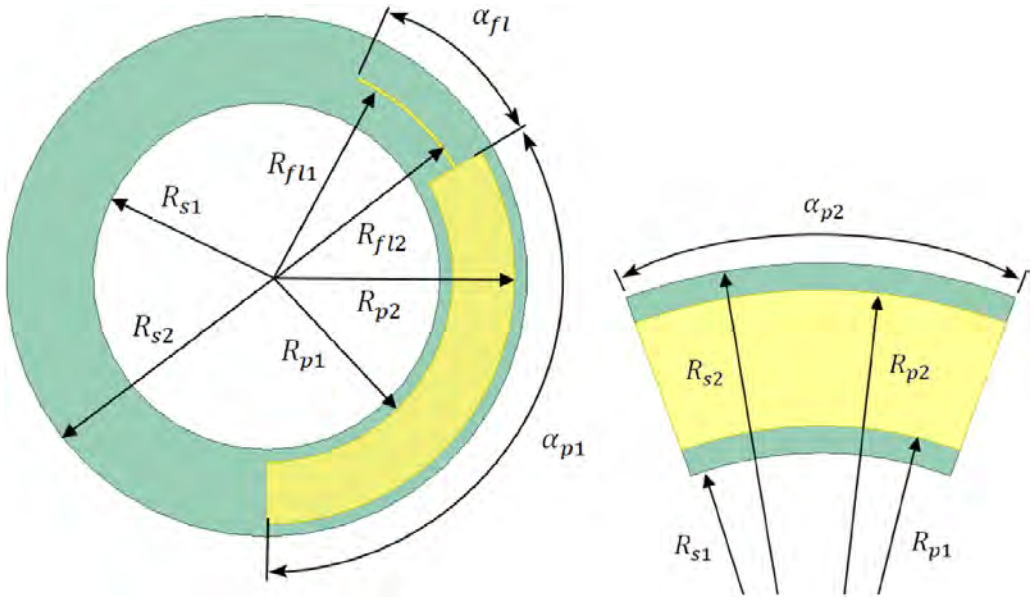

Figure 4. A schematic diagram of each parameter.

equivalent radius of the sector ring patch (R) in equation (3) can be determined, and its value is 34.14 mm. Further, the relationship between the third-order resonant frequency and the overlapping angle between Patch 1 and Patch 2 can be deduced according to theoretical equation (2), shown by the green curve in figure 7 with a correlation coefficient of 0.9970.

In addition, according to equation (5), when the circumferential length of the equivalent radiation patch of the antenna changes slightly, the antenna's resonant frequency changes linearly with the change in peripheral length. The change in the equivalent peripheral length of the equivalent radiation patch is controlled by the change of the overlapping angle between Patch 1 and Patch 2.

To test this hypothesis, the overlapping angle varies from 35° to 40° with a 0.5° per step, and the relationship between the resonant frequency and the overlapping angle is obtained and shown in figure 8. Through linear fitting of the simulation

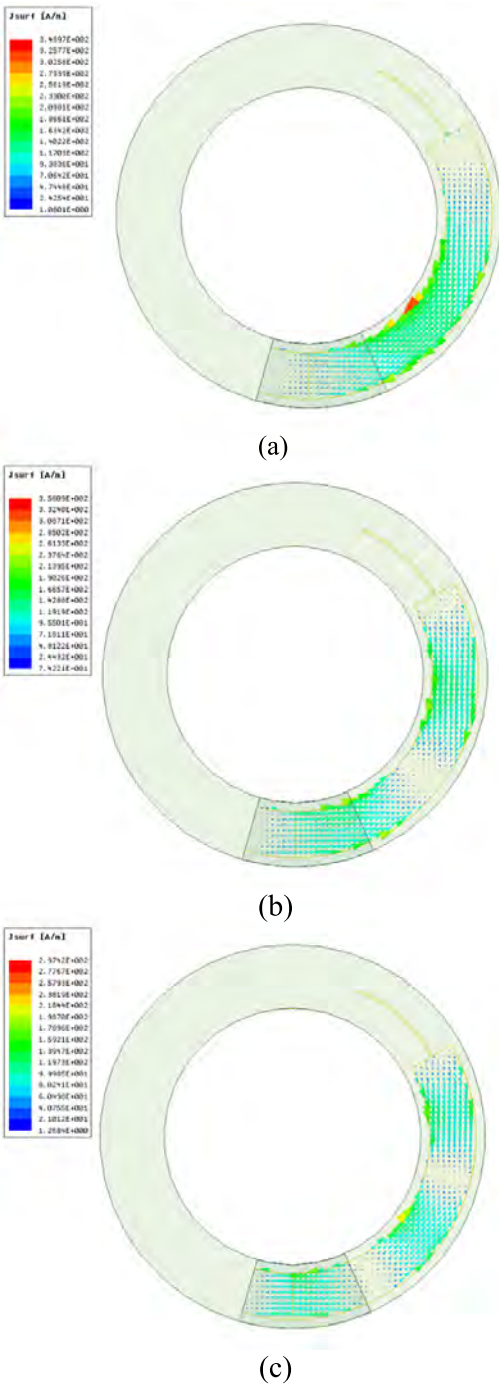

Figure 5. Current distribution diagrams of the first three SRPA resonances. (a) The first-order resonance, (b) the second-order resonance, and (c) the third-order resonance.

results, the antenna's sensitivity is 23.3 MHz per degree, and the correlation coefficient is 0.9973. Further, to simulate the performance of the SRPA in practice, a steel block is added near the sensor in HFSS. With other setting unchanged, the simulation results are shown in figure 9. The sensitivity is 21.9 MHz per degree, and the correlation coefficient is 0.9982. The presence of the steel block has little effect on the performance of the sensor, and only slightly reduces the sensitivity of SRPA.

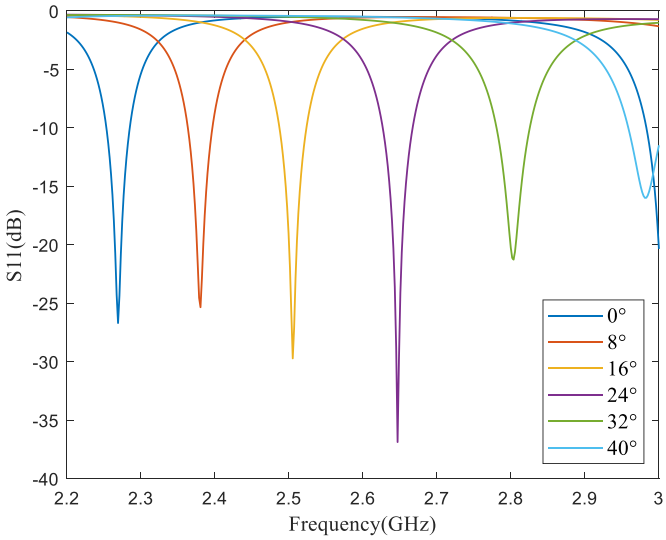

Figure 6. The S11 curves of simulation.

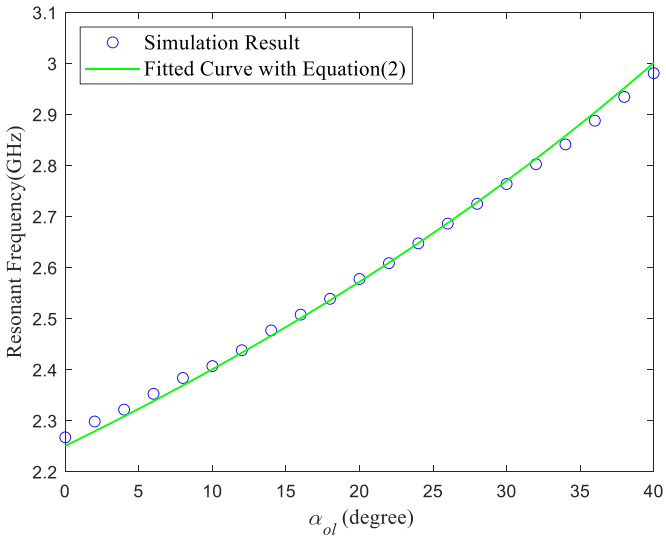

Figure 7. Relationship between α_{ol} and resonant frequency.

Due to the differences between the actural application and simulation in surrounding environment, boundary conditions, etc, experiment are still necessary to verify the practicality of the sensor.

3.3. Temperature and humidity effects

In practical application, the influence of temperature and humidity on the SRPA needs to be considered. As for the humidity effect on the antenna's characteristics, according to Jain *et al* [27], humidity has a significant effect on the reflection coefficient of the antenna but has little effect on the resonant frequency of the antenna. And Hertleer *et al*'s [28] study showed that the antenna's performance is relatively stable when the moisture absorption rate of substrate is less than 3%. In contrast, the typical value of the moisture absorption rate of FR4 used in SRPA is only 0.2%.

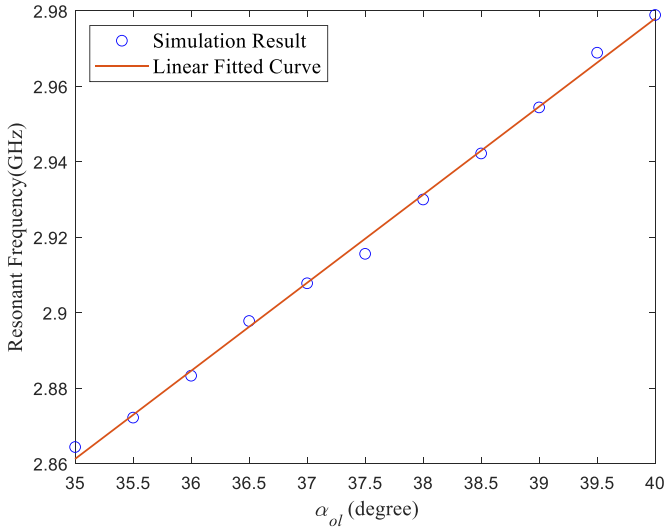

Figure 8. Relationship between the overlapping angle and the resonant frequency.

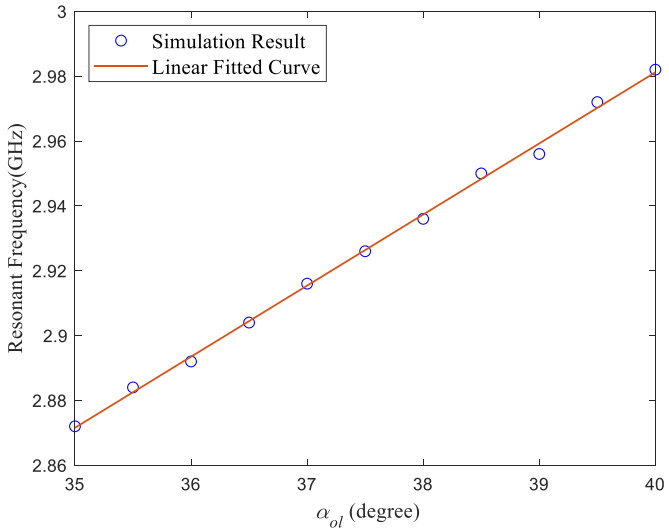

Figure 9. The relationship between the overlapping angle and the resonant frequency when there is a steel block near SRPA.

Temperature affects the resonant frequency of an antenna mainly by affecting the dielectric constant of the substrate. The relationship between the dielectric constant of the substrate and the surrounding temperature can be expressed by the thermal coefficient of dielectric constant (TCDk). FR4's TCDk is typically -200 parts per million (ppm) per degree celsius (°C). Because of it, temperature compensation can be achieved by establishing the relationship between the resonant frequency and temperature change. According to equation (2), assuming that the antenna operates at 3 GHz, a temperature change of 1° Celsius will cause a 0.6 MHz antenna frequency change when using FR4 material with TCDk -200 ppm °C^{-1} as the substrate. In addition, ITEQ CORPORATION has developed a new FR4-based substrate material IT-8338 A and IT-8350 A with TCDk of -35 ppm °C^{-1}. In order to reduce the influence of temperature on the resonant frequency of the antenna, the substrate of SRPA in practical application can be made of this new material. The actual ambient temperature range in civil engineering is about 70 °C. When using FR4 material with TCDk -35 ppm °C^{-1} as substrate and the antenna is operating at 3 GHz frequency, a temperature change of 70 °C causes the resonant frequency of SRPA to change about 3.0 MHz by theoretical calculation. According to the simulation results, the resonant frequency of SRPA changes up to 23.3 MHz when the nut rotates one degree. At this point, the effect of temperature change on the resonant frequency of the SRPA is not relevant or even can be ignored.

In conclusion, humidity has little influence on the resonant frequency of the SRPA. And the effect of temperature on resonant frequency can be solved by temperature compensation or an alternative substrate made of temperature-insensitive materials. Therefore, these two factors are not considered in the practical experiments.

4. Experiment

For experiments, we made two sets of SRPAs with the same dimensions as designed in the simulation section. Copper was selected as the material used to fabricate all the printed patches and the feed line, and FR4 was used for making the substrates.

4.1. Instrumentation setup

To verify the simulation results and the performance of the antenna in practical application, two sets of antennas with the same parameters were tested. The instrumentation setup was established, as shown in figure 10.

For simulating the actual working environment of the SRPA and to obtain a better way to work on and affix the bolt, a steel block was made. The central opening was used to fix the M24 bolt for testing. The paper with scales was printed and pasted to the ring substrate of the SRPA to control the rotation angle of the sector ring substrate during the test. After the M24 bolt was fixed on the steel block, the ring substrate was pasted on the steel block to ensure that the center of the ring substrate coincided with the center of the M24 bolt's screw. The sector ring substrate was then attached to the nut through a connection with a hexagonal opening. The rotation of the sector ring substrate can be controlled by controlling the rotation of the nut, and the specific rotation angle can be controlled by the paper with scales pasted on the ring substrate. The SRPA was connected to a vector network analyzer (VNA) via a coaxial line. And the function of the VNA is to obtain the S11 curve of the antenna.

At the start of the test, Patch 1 is in contact with Patch 2 ($\alpha_{ol} = 0$); then, the sector ring substrate rotated clockwise along the ring substrate with a 2° per step until the two patches were overlapped completely. The VNA sent a sweeping signal from 2 GHz to 3 GHz to the SRPA and monitored the backscattering signal from the antenna to obtain the S11 curve for each step. Data acquisition by the VNA occurred after a 30 s stabilization period to enhance the quality of the data. From S11 curve, the SRPA's resonant frequencies of each step

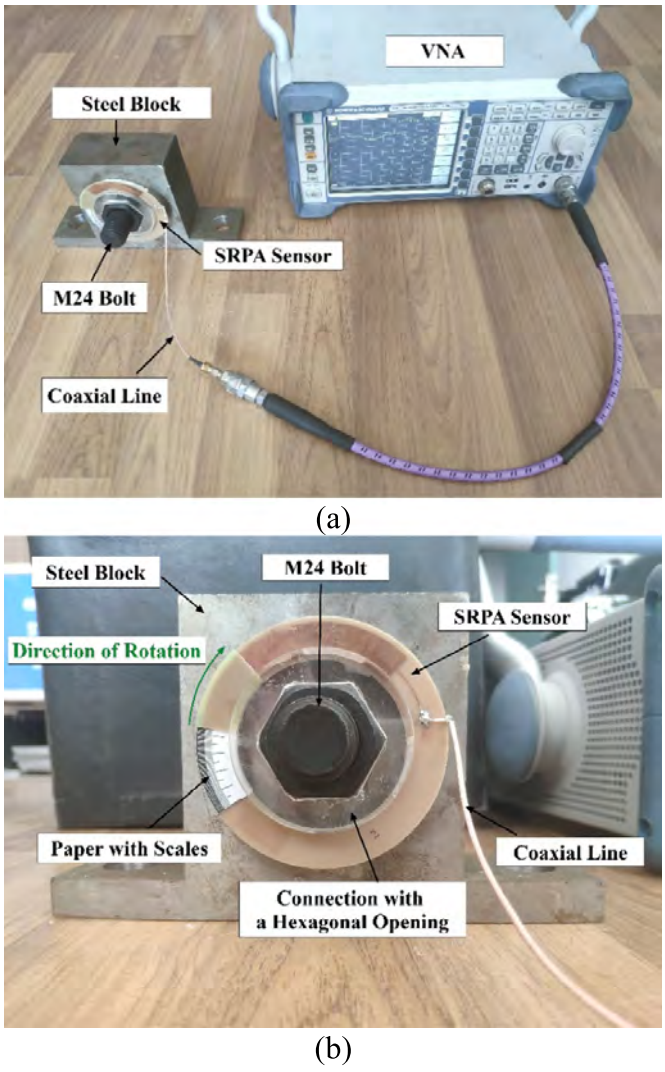

Figure 10. Instrumentation setup. (a) The SRPA connected to the VNA and (b) the SRPA fixed on the steel block.

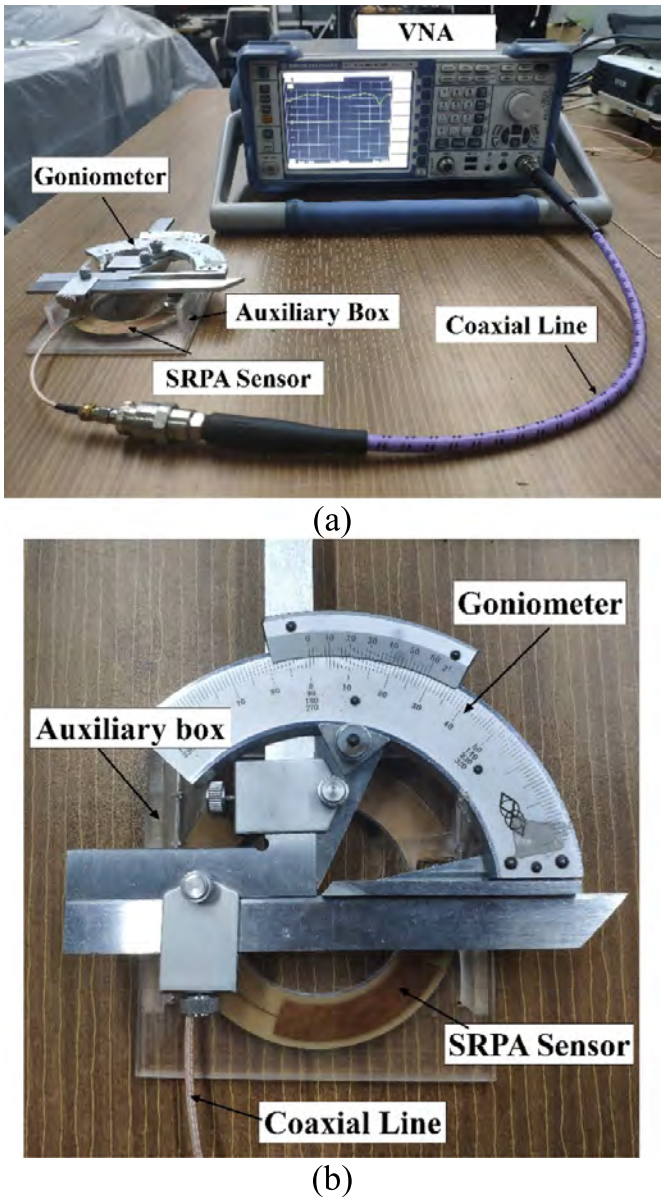

Figure 11. Instrumentation setup for precise control. (a) The SRPA connected to the VNA and (b) the SRPA and goniometer fixed on the auxiliary box.

were extracted, and further, the resonant frequency shift was obtained.

To verify where there is a linear relationship between the resonant frequency and the overlapping angle when the change of the overlapping angle is small, we designed a new experimental instrumentation setup to more accurately control the relative rotation between Patch 1 and Patch 2, as shown in figure 11. The auxiliary box, ring substrate and goniometer were relatively fixed, and the sector ring substrate was relatively fixed to the rotatable part of the goniometer. By controlling the rotating part of the goniometer, the relative rotation of Patch 1 and Patch 2 can be controlled precisely. Because the overlapping angle between Patch 1 and Patch 2 varies from 35° to 40° with 1/6 degree per step, the S11 curve of the antenna was recorded.

4.2. Experimental results

The relationship between the resonant frequency of the SRPA and the overlapping angle between Patch 1 and Patch 2 obtained from the tests are shown in figure 12. According to the test results, the effective radius of the first group and the second group of the sensors are 35.14 mm and 35.35 mm, respectively. The theoretical curves between the resonant frequency and overlapping angle corresponding to the two sets of sensors derived from equation (2) are also drawn in figure 12, whose correlation coefficients are severally 0.9942 and 0.9974.

The equivalent radius R of the sensor obtained from the simulation and the test is different because of the different environments between the simulation and the actual test. In addition, the slight difference in the equivalent radii of the two sets of sensors may be caused by a manufacturing or operation error.

When the overlapping angle changes from 35° to 40°, the relationship between the antenna resonant frequency and the

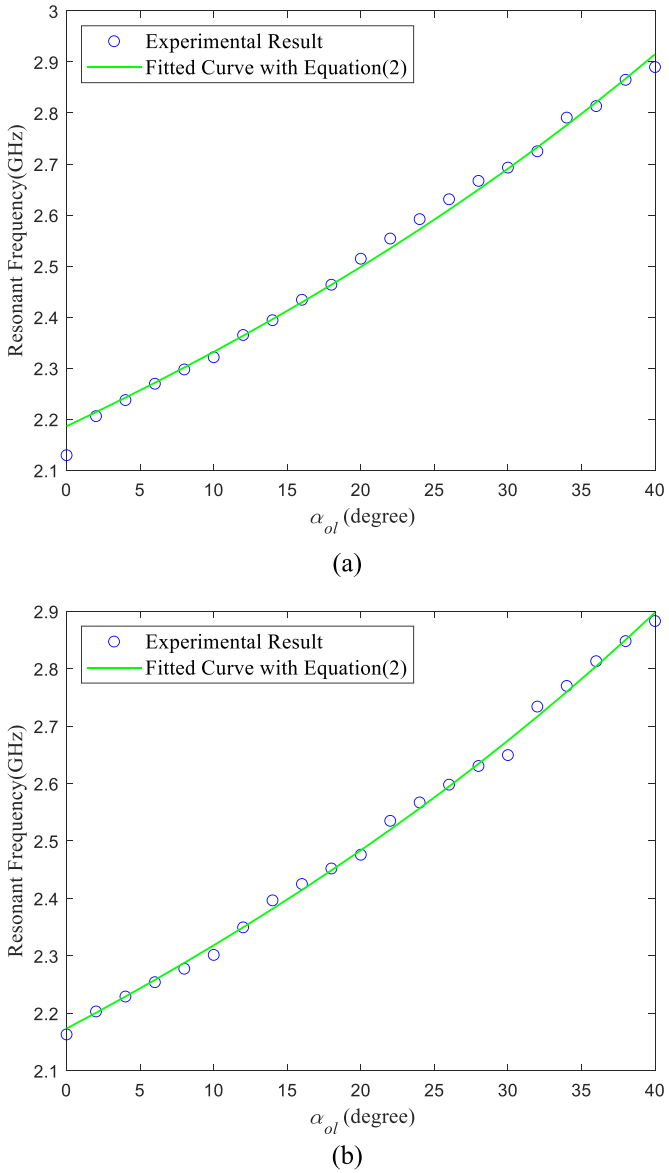

Figure 12. Relationship between the resonant frequency and the overlapping angle. (a) Group 1 and (b) group 2.

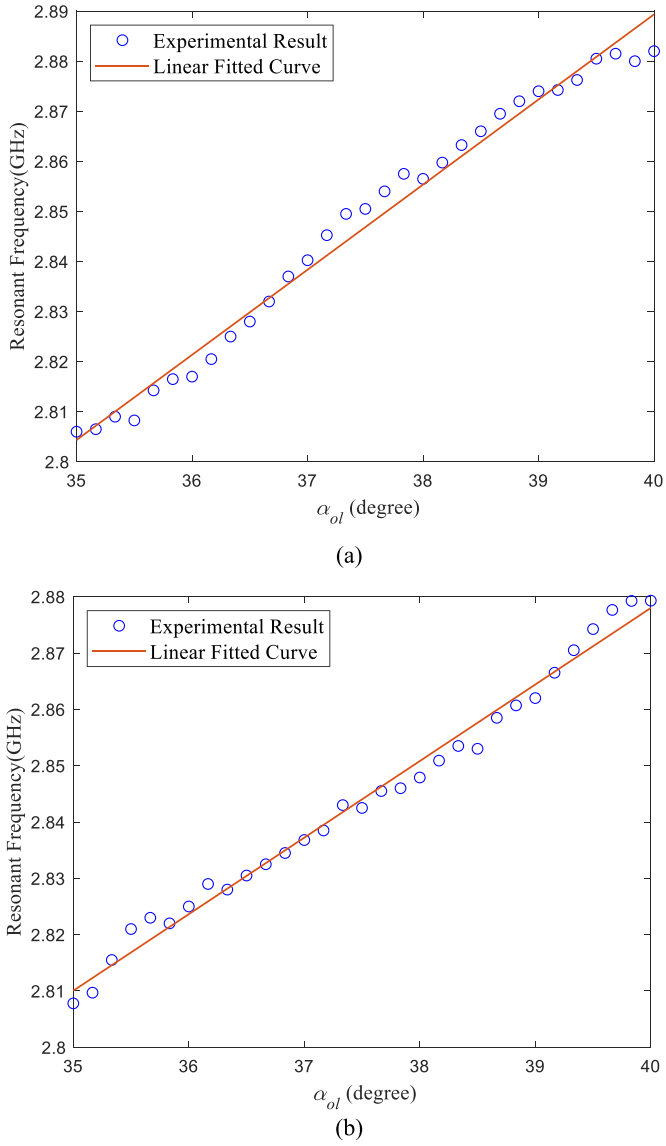

Figure 13. Relationship between the overlapping angle and the resonant frequency. (a) Group 1 and (b) group 2.

overlapping angle is shown in figure 13. MATLAB is used for linear fitting of experimental data. According to the fitting results, the sensitivities of the two groups of antennas are 17.3 MHz per degree and 14.3 MHz per degree, with the correlation coefficients of 0.9886 and 0.9897, respectively.

5. Results' comparison and discussion

The results of the numerical simulation and experiment are shown in table 2. The equivalent radius was obtained by fitting the relationship between the overlapping angle and the resonant frequency with equation (2) in the range of 0° to 40° of the overlapping angle. The sensitivity is derived by linear fitting of the simulation results and experiment results when the overlapping angle changes between 35° and 40° degrees. And these two correlation coefficients on each line correspond to the correlation coefficients of the equation fitting and linear fitting, respectively.

For simulation results and experimental results, both results are consistent with the theory in the range of 0°–40°of the overlapping angle between Patch 1 and Patch 2. These results indicate a great linear relationship exists between the overlapping angle of Patch 1 and Patch 2 and the resonant frequency when the overlapping angle changes between 35° and 40°. However, compared with the simulation results, the experimental results have larger equivalent radius and lower sensitivity. Those differences are probably due to the following reasons:

(a) In the experiment, there are welding of the feeding point and environmental interference, which are not considered in the simulation.
(b) In the simulation, the connection between Patch 1 and Patch 2 can be considered as an air-tight connection.

Table 2. Simulation results and experiment results.

		Equivalent radius (mm)	Sensitivity (MHz per degree)	Correlation coefficients (equation/linear fitting)
Simulation		34.14	23.30	0.9970/0.9973
Experiment	Group1	35.14	17.30	0.9942/0.9886
	Group2	35.35	14.30	0.9974/0.9897

However, in the experiment, there is always an air film between the two patches; thus, a tight connection is impossible to achieve.

(c) Fabrication errors. The antenna substrates or patches are not completely flat, and the dimensions are also subject to some errors between the actual antenna and the design.

(d) The centers of the two substrates do not coincide entirely in the actual test, which is also different from the simulation.

When used for bolt loosening monitoring, it is sufficient to select the case where the overlapping angle varies between 35° and 40° because the bolt has already loosened when the nut produces a relatively small rotation. In this case, the relationship between the resonant frequency and the overlapping angle can be seen as linear, making the sensor easier to calibrate in practice. And according to the experiment in this paper, the angle sensor can measure the minimum angle change of 1/6 degree, which allows us to detect early bolt loosening in a timely manner.

In addition to bolt loosening detection, the angle sensor is also suitable for a wide range of angle changes. The maximum measurement range of the sensor proposed in this paper is 40°. By optimizing the dimensions, this form of sensor can support a larger measurement range.

6. Conclusions

In this paper, the authors introduced a SRPA sensor for bolt loosening detection. The resonant cavity theory was applied to explain the relationship between the resonant frequency and the overlapping angle of Patch 1 and Patch 2. The optimal dimensions of the antenna were tested in a wired-testing environment. The experimental results are consistent with the simulation results and the theoretical analysis. The experimental results show that the relationship between the antenna resonant frequency and the overlapping angle is consistent with the theoretical equation when the overlapping angle varies from 0° to 40°. In case of small changes in the overlapping angle, the antenna's resonant frequency changes linearly with the change of the overlapping angle. The SRPA has a sensitivity of 15.8 MHz per degree on average and can detect a 1/6° bolt rotation minimally within the range of the overlapping angle from 35° to 40°.

Data availability statement

The data generated and/or analysed during the current study are not publicly available for legal/ethical reasons but are available from the corresponding author on reasonable request.

Acknowledgments

Funding: This research was funded by the National Natural Science Foundation of China (Grant Nos. 52078375 and 52178298) and the Key Program for International S&T Cooperation Projects of China (No. 2021YFE010033).

ORCID iDs

Zhiquan Zheng https://orcid.org/0000-0002-6592-3960
Liyu Xie https://orcid.org/0000-0001-5777-0645
Guochun Wan https://orcid.org/0000-0003-0521-1176

References

[1] Nikravesh S M Y and Goudarzi M 2017 A review paper on looseness detection methods in bolted structures *Lat. Am. J. Solids Struct.* **14** 2153–76

[2] Huynh T C, Park J H, Jung H J and Kim J T 2019 Quasi-autonomous bolt-loosening detection method using vision-based deep learning and image processing *Autom. Constr.* **105** 102844

[3] Wang F and Song G 2020 Bolt-looseness detection by a new percussion-based method using multifractal analysis and gradient boosting decision tree *Struct. Health Monit.* **19** 2023–32

[4] Bickford J H 2007 *Introduction to the Design and Behavior of Bolted Joints* ed J H Bickford (Boca Raton, FL: CRC Press) (https://doi.org/10.1201/9780849381874)

[5] Kim N and Hong M 2009 Measurement of axial stress using mode-converted ultrasound *NDT&E Int.* **42** 164–9

[6] Huynh T C, Dang N L and Kim J T 2018 Preload monitoring in bolted connection using piezoelectric-based smart interface *Sensors* **18** 18–22

[7] Wang C, Wang N, Ho S C, Chen X, Pan M and Song G 2018 Design of a novel wearable sensor device for real-time bolted joints health monitoring *IEEE Internet Things J.* **5** 5307–16

[8] He K and Zhu W D 2014 Detecting loosening of bolted connections in a pipeline using changes in natural frequencies *J. Vib. Acoust.* **136** 1–8

[9] Park J H, Kim T H and Kim J T 2015 Image-based bolt-loosening detection technique of bolt joint in steel bridges *Int. Conf. on Advances in Experimental Structural Engineering (August 2015)*

[10] Razi P, Esmaeel R A and Taheri F 2013 Improvement of a vibration-based damage detection approach for health monitoring of bolted flange joints in pipelines *Struct. Health Monit.* **12** 207–24

[11] Yang J and Chang F K 2006 Detection of bolt loosening in C-C composite thermal protection panels: I. Diagnostic principle *Smart Mater. Struct.* **15** 581–90
[12] Wang T, Song G, Wang Z and Li Y 2013 Proof-of-concept study of monitoring bolt connection status using a piezoelectric based active sensing method *Smart Mater. Struct.* **22** 087001
[13] Suda M, Hasuo Y, Kanaya A, Ogura Y and Takishita Y S 1992 Development of ultrasonic axial bolting force inspection system for turbine bolts in thermal power plants *JSME Int. J.* 1 **35** 216–9
[14] Barbieri E, Meo M and Polimeno U 2009 Nonlinear wave propagation in damaged hysteretic materials using a frequency domain-based PM space formulation *Int. J. Solids Struct.* **46** 165–80
[15] Ramana L, Choi W and Cha Y J 2019 Fully automated vision-based loosened bolt detection using the Viola–Jones algorithm *Struct. Health Monit.* **18** 422–34
[16] Wu J, Cui X and Xu Y 2016 A novel RFID-based sensing method for low-cost bolt loosening monitoring *Sensors* **16** 1–15
[17] Songtao X, Zheng Z, Guan S, Xie L, Wan G and Wan C 2020 A capacitively-fed inverted-F antenna for displacement detection in structural health monitoring *Sensors* **20** 5310
[18] Xue S, Jiang K, Guan S, Xie L, Wan G and Wan C 2020 Long-range displacement meters based on chipped circular patch antenna *Sensors* **20** 4884
[19] Daliri A, Galehdar A, Rowe W S T, Ghorbani K and John S 2012 Utilising microstrip patch antenna strain sensors for structural health monitoring *J. Intell. Mater. Syst. Struct.* **23** 169–82
[20] Yi X, Wu T, Wang Y and Tentzeris M M 2015 Sensitivity modeling of an RFID-based strain-sensing antenna with dielectric constant change *IEEE Sens. J.* **15** 6147–55
[21] Yi X, Cho C, Cooper J, Wang Y, Tentzeris M M and Leon R T 2013 Passive wireless antenna sensor for strain and crack sensing—electromagnetic modeling, simulation, and testing *Smart Mater. Struct.* **22** 085009
[22] Yi Z, Xue S, Xie L and Wan G 2021 Detection of setting time in cement hydration using patch antenna sensor *Struct. Control Health Monit.* **29** e2855
[23] Xue S, Xu K, Xie L and Wan G 2019 Crack sensor based on patch antenna fed by capacitive microstrip lines *Smart Mater. Struct.* **28** 085012
[24] Xue S, Yi Z, Xie L, Wan G and Ding T 2019 A passive wireless crack sensor based on patch antenna with overlapping sub-patch *Sensors* **19** 4327
[25] Xue S, Li X, Xie L, Yi Z and Wan G 2021 A bolt loosening detection method based on patch antenna with overlapping sub-patch *Struct. Health Monit.* 1–13
[26] Balanis C A 2016 *Antenna Theory: Analysis and Design* (New York: Wiley)
[27] Jain S, Mishra K P, Thakare V V and Mishra J 2018 Microstrip moisture sensor based on microstrip patch antenna *Prog. Electromagn. Res.* M **76** 177–85
[28] Hertleer C, van Laere A, Rogier H and van Langenhove L 2010 Influence of relative humidity on textile antenna performance *Text. Res. J.* **80** 177–83